Proceedings of the ASME 2010 3rd Joint US-European Fluids Engineering Summer Meeting and 8th International Conference on Nanochannels, Microchannels, and Minichannels
FEDSM-ICNMM2010
August 1-5, 2010, Montreal, Canada

FEDSM-ICNMM2010-30808

WIND TUNNEL STUDIES ON THE GALLOPING OF LIGHTLY-ICED TRANSMISSION LINES

Patrick H. Fleming
Department of Mechanical and Manufacturing Engineering
University of Manitoba
Winnipeg, MB, Canada
Email: umflemi5@cc.umanitoba.ca

Neil Popplewell*
Department of Mechanical and Manufacturing Engineering
University of Manitoba
Winnipeg, MB, Canada
Email: npopple@cc.umanitoba.ca

ABSTRACT

The aerodynamics involved in the galloping of lightly-iced transmission lines were studied in a series of wind tunnel experiments. A representative section of a lightly-iced conductor produced in an outdoor freezing rain simulator was used throughout. In the first set of experiments aerodynamic loads were measured on a static model at different wind speeds and angles of attack. These experiments showed that the well-established den Hartog criterion does not predict an instability at wind speeds associated with transmission line galloping. A second set of experiments examined the effects of different steady rotational motions on the aerodynamic loads. Automated controls were used to rotationally oscillate the model in a repeatable manner at various angles of attack and rotational amplitudes as well as frequencies. The drag remained consistent with quasi-steady values, while the lift was affected by the rotational motion. This rotation-induced lift was enhanced by ice surface irregularities, but further studies were needed to fully assess its importance.

INTRODUCTION

Overhead transmission lines are prone to experience high amplitude, low frequency vibrations when exposed to freezing rain and sustained winds. This specific type of wind-induced vibration has been observed and studied since about the start of the electric power industry, and is commonly referred to as galloping. Field reports show that galloping lines may reach vertical amplitudes up to 15m, peak-to-peak (p-p), at frequencies of about 0.1 to 0.5Hz [1]. In addition to a dominant vertical motion, galloping transmission lines also have a tendency to sway horizontally, up to 3m (p-p) [2], and twist up to about 40 degrees, with a rotational frequency of 1 to 8 times the vertical galloping frequency [3,4]. These vertical, horizontal, and rotational motions may severely damage support hardware and towers, and disrupt electrical service. Economic factors, as well as the multifaceted nature of the problem, provide motivation for the study and research of galloping transmission lines.

Detailed data for cases of natural iced transmission line galloping in the field are not available. The ice shape and twisting motion of a single galloping conductor line are very difficult to observe, let alone measure from the ground. In the absence of detailed field data, general visual reports [1] and full-scale field tests [3-5] have played an important role in identifying the characteristics of iced transmission line galloping. For example, North American field reports show two important trends: lightly-iced lines, or lines with a maximum ice thickness of 10% or less of the bare conductor's diameter, are the most prone to gallop [1]; and steady winds of about 5-15m/s are the most common wind conditions for galloping [5,6]. Of these two trends, the former is the most significant as transmission line galloping associated with thin ice shapes has not yet been explained satisfactorily. The present work addresses this issue by focusing solely on galloping of lightly-iced transmission lines.

BACKGROUND

Most of the previous wind tunnel studies on transmission line galloping have used either static or spring-supported models [2, 7-11]. Based on quasi-steady theory and aerodynamic data from static models, Tunstall [12] and Richardson [13] have argued that typical lightly-iced conductor profiles satisfy den Hartog's criterion [14] for purely vertical

* Address all correspondence to this author.

galloping. Den Hartog's criterion is

$$\frac{\partial L}{\partial \alpha} + D < 0 \tag{1}$$

where α is the angle of attack and L and D are the aerodynamic lift and drag forces, respectively. Negative aerodynamic damping and vertical galloping may occur when the criterion is satisfied. In contrast, Ontario Hydro [8,9] showed that iced-conductor models supported by springs, but restrained to move only vertical direction, are vertically stable, and that rotational motion plays a significant role. Similarly, the numerical simulations by McComber and Paradis [15] emphasise a rotation-induced lift mechanism, although no experiments were performed. This general disagreement in the literature demonstrates that the aerodynamics involved in the problem are not yet well understood. Additional research on the rotational effects and aerodynamics acting in transmission line galloping is warranted. The present study uses a forced-vibration method as it is complementary to the previous work involving static and spring-supported models.

In comparison to 1-degree-of-freedom (DOF) vertical galloping, relatively few studies have been conducted on 1-DOF rotational galloping. This may be due to the more complicated aerodynamic nature and its controversial role in galloping. Indeed the corresponding aerodynamic moment acting in rotational galloping is very small in magnitude and, hence, it is usually difficult to measure experimentally [16]. As early as 1950, however, Cheers [17] suggested that rotational instability may be much more influential in iced transmission galloping than the vertical den Hartog mechanism. The influence of difficult to observe rotations in the field galloping of iced transmission lines still remains unresolved. The extension of the quasi-steady theory to the rotational DOF for a lightly-iced conductor profile requires further discussion and consideration due to its possible important role.

Quasi-steady theory and the den Hartog criterion are based on static aerodynamic data. The quasi-steady theory implies that a stationary and a moving galloping structure experience the same aerodynamics loads, if they both have the same effective angle of attack, α_{eff}, and wind speed, V_{eff}. As shown in Fig. 1(a) for the case of 1-DOF vertical galloping, the effective wind speed and angle of attack depend on the vertical velocity of the galloping structure, $\dot{y}$, and the actual wind speed, V. For the rotational case shown in Fig. 1(b), the effective wind speed and angle of attack are assumed to depend on three parameters: a characteristic radius, r, sometimes taken as half the bare conductor diameter, d [18]; the galloping or fluttering structure's rotational velocity, $\dot{\theta}$; and the actual wind speed, V [19]. Experiments [16, 20-22] involving ideal ice shapes or rectangular prisms show that quasi-steady aerodynamics for rotational motion are of limited practical use. Quasi-steady theory, even with the use of a characteristic radius, oversimplifies the complex phase or "fluid-memory" effects between the aerodynamic moment and rotational displacement [20]. Despite these findings from rectangular prisms, numerical models for simulating iced transmission line galloping [18,23] have adopted the quasi-steady theory to account for rotational effects. Wind tunnel experiments with a representative model of a lightly-iced conductor are needed to improve these numerical models. Such experiments provide a better understanding of how a rotational motion affects the aerodynamic loads in transmission line galloping.

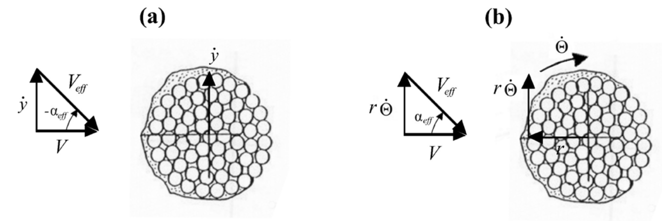

FIGURE 1. QUASI-STEADY MODELLING FOR (a) VERTICAL GALLOPING AND (b) ROTATIONAL GALLOPING.

EXPERIMENTAL APPARATUS

Wind Tunnel

The wind tunnel used for the present study is a return-circuit type with an octagonal test section measuring 53H x 76W x 183L cm. The corner fillets of the test section gradually taper to account for boundary layer growth. Wind speeds of 0-30m/s can be produced in the test section, with a turbulence intensity level of less than about 0.3% at 20m/s, respectively. The wind speed is checked by monitoring the static pressure drop across the contraction cone upstream of the test section. A wind speed controller is also equipped with additional automation equipment to account for changes in solid blockage due to changes in a model's angle of attack. This automation system relieves the wind tunnel operator of having to perform tedious wind speed adjustments at each angle of attack considered in a quasi-steady (static) test.

Lightly-Iced Conductor Model

The model used in the present experiments is a plaster replica of a lightly-iced conductor. Figure 2 shows the model's cross-sectional shape and the coordinate system for the aerodynamic measurements, where θ is the rotational position of the model. The original iced sample was produced in an outdoor freezing rain simulator with a 28.6mm diameter conductor [24]. The replica model is full-scale in its cross-sectional geometry and measures 52.6cm in length, giving a length to diameter ratio of about 21:1. The model is orientated vertically and spans almost the entire height of the test section, leaving approximately 2mm gaps at the upper and lower surfaces. The present arrangement yields comparable aerodynamic data to a 50:1 iced-conductor model fitted with end plates in the National Research Council's (NRC) 2x3m wind tunnel [25].

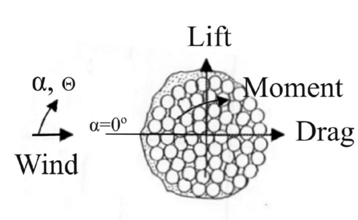

FIGURE 2. COORDINATE SYSTEM AND CROSS-SECTIONAL SHAPE OF A TYPICAL LIGHTLY-ICED CONDUCTOR.

The vertical model configuration is useful for studying the simplest case of transmission line galloping caused by a steady, perpendicular side wind. Although recent field testing [5] has confirmed that galloping may occur in non-perpendicular winds, previous wind tunnel experiments suggest that yaw effects have no appreciable change on galloping instability [7]. As an additional constraint, the effects of turbulence are not considered here as large turbulent scales inherent to atmospheric wind cannot be produced in wind tunnels. However, Tunstall [12] has argued that grid-generated wind tunnel turbulence, characterised by length scales having the same order of magnitude as the conductor diameter, is less representative than uniform, low-turbulent flow conditions for studying galloping in wind tunnels. The present experiments are therefore limited to smooth, low-turbulent wind conditions.

Aerodynamic Balance and Automated Controls

The aerodynamic balance used in the present experiments is a general-purpose, six-component Aerolab pyramidal balance. The balance has been retrofitted with new strain gauges and more sensitive load cells, as the aerodynamic lift and moment associated with lightly-iced conductors are very small in magnitude [24]. In addition, the balance has been integrated with automated controls for static and dynamic testing involving purely rotational motion. The automation hardware is made up of a stepper motor and driver, an incremental encoder, and a motion controller card for a personal computer. The system is closed-loop and can achieve an absolute accuracy of ±0.2°. The motion controller card, when programmed appropriately, provides arbitrary path-controlled motion abilities for forced-vibration studies involving a solely 1-DOF rotational motion.

Laser-Based Visualisation

Previous studies on rotationally-oscillating cylinders [26], flutter [21], and iced-conductor galloping [27] have all used the smoke-wire visualisation technique to complement aerodynamic data. Visualisation experiments were planned also in the present study to help interpret data from the aerodynamic balance. However, the previous studies noted above used wind speeds of about 1-3m/s, and at a realistic galloping wind speed of about 10m/s, the smoke-wire technique is not feasible [26,28]; an alternative visualisation system based on readily available components for particle-image velocimetry (PIV) is used instead.

The visualisation system for the present study uses di-ethyl hexyl sebacate (DEHS) oil droplets, as they are one of the most commonly used tracer particles for PIV in air [28]. The tracer particles are generated using two laskin-nozzle devices and dispensed into the wind tunnel upstream of the contraction cones and flow conditioning screens to minimise flow disturbance. As the tracer particles follow the airflow around the wind tunnel model, they are illuminated by a 1mm horizontal light sheet generated from a 5W continuos Argon:Ion laser. The light sheet is located at the midheight of the test section and the wind tunnel model. The streamlines around the wind tunnel model are recorded using a Dantec MKIII Nanosense camera set at a frame rate of 200Hz.

EXPERIMENTAL DETAILS

The experiments for the present study are organised into three types: quasi-steady testing involving a stationary model, dynamic testing involving a 1-DOF rotationally-oscillating model, and visualisation experiments.

Quasi-Steady Experiments

Quasi-steady or stationary testing involves characterising the aerodynamics resulting from the airflow around a static model. The model's angle of attack is generally varied incrementally and, at each angle of attack considered, the aerodynamic loads acting on the static model are measured. In a previous quasi-steady experiments involving iced-conductor models, a relatively high wind speed of 30m/s was used [24]. Although such a high wind speed is not realistic for galloping transmission lines, this approach was taken to increase the signal-to-noise ratios involved in the aerodynamic load measurements. Furthermore, for moderately iced conductors, experiments conducted at 10 and 30m/s gave fairly similar results for the normalised aerodynamic lift, drag, and moment coefficients, C_L, C_D, and C_M, respectively [29]. The normalised aerodynamic coefficients are defined as

$$C_L = \frac{L}{\frac{1}{2}\rho V^2 d l} \tag{2}$$

$$C_D = \frac{D}{\frac{1}{2}\rho V^2 d l} \tag{3}$$

$$C_M = \frac{M}{\frac{1}{2}\rho V^2 d^2 l} \tag{4}$$

where ρ is the density of air, M is the aerodynamic moment, and d and l are the model's bare conductor diameter and length, respectively. Results from the quasi-steady experiments are plotted as aerodynamic coefficients versus angle of attack curves.

In the present quasi-steady experiments, realistic wind speeds of 10, 14, and 18m/s are examined for the model shown in Fig. 2. The angle of attack for each wind speed is varied from 0 to 360° in increments of 2°. The 360° range is considered here for completeness, as well as to include the case of a wind reversal, where the wind reverses its direction after the icing process, resulting in an angle of attack around 180°[2]. At each angle of attack, 2000 data samples of the aerodynamic loads are recorded at a sampling rate of 2000 samples per second, and the average of the 2000 samples is computed. Longer sample durations of 5s were considered in preliminary trials, but yielded similar averages compared to data collected over 1s. The closed-loop motion control hardware as well as the wind speed controller were used to automatically position the model and maintain a constant wind speed.

Forced-Vibration Experiments

Forced-vibration experiments involve the wind tunnel model undergoing controlled, steady rotational oscillations. The model's rotational position as a function of time, t, is given in Eqn. 5.

$$\theta = \alpha_0 + A_\theta \cos(2\pi f_\theta t) \tag{5}$$

where the initial angle of attack, α_0, oscillation amplitude, A_θ, and frequency, f_θ, are varied in the programming of the motion control card. The period of oscillation, $T_\theta = 1/f_\theta$, is used later when presenting results in a non-dimensional form. Figure 3 shows an example of the model's repeatable motion. As the model oscillates, the unsteady aerodynamic loads are measured by employing the aerodynamic balance's load cells. The same model and vertical orientation as that for the quasi-steady testing are used in these dynamic tests. Therefore, the quasi-steady aerodynamic measurements serve as a baseline for the results from the forced-vibration tests. The key parameters varied during the dynamic experiments are the model's initial angle of attack, and the steady-state amplitude and frequency of the model's rotational oscillation.

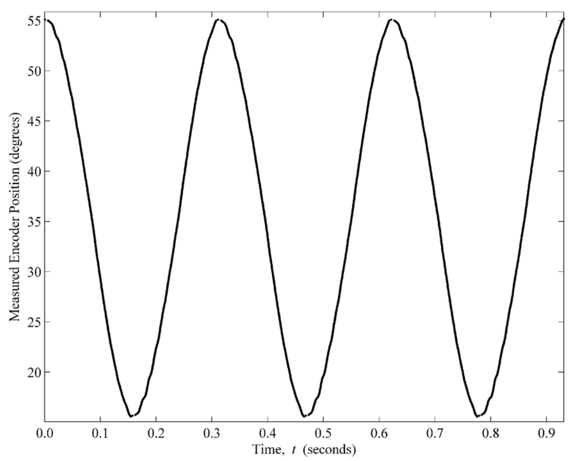

FIGURE 3. REPEATABLE MOTION OF THE WIND TUNNEL MODEL MEASURED USING AN INCREMENTAL ENCODER.

Visualisation Experiments

Visualisation experiments are described next for the previous quasi-steady and forced-vibration tests. Only the most significant results are given due the shear volume of images produced by the visualisation technique.

Due to the use of only one laser and camera, the wind tunnel model's two separation points cannot be visualised simultaneously. The model's second separation point, which is located opposite to the laser is not illuminated due to the model blocking the laser sheet. To simultaneously capture both separation points, two cameras are needed as well as costly additions to the laser's optics so that multiple light-sheets can be projected. As the automated controls provide repeatable motions, an alternative arrangement is to conduct two visualisation experiments. The first experiment would capture one of the model's two separation points. In the second experiment, the model would undergo the same motion, but it is rotated to a new initial angle of attack to enable the second separation point to be illuminated by the laser. Figure 4 illustrates these two experiments. As lightly-iced conductor models are nearly symmetrical, and the flow in the wind tunnel is uniform, conducting these two separate visualisation experiments is expected to produce comparable results to simultaneously capturing both separation points.

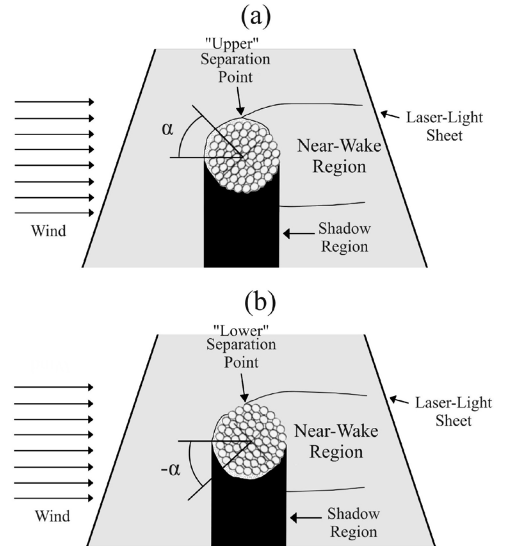

FIGURE 4. ILLUSTRATION OF EXPERIMENTS TO VISUALISE (a) "UPPER" AND (b) "LOWER" SEPARATION POINTS.

FORCED-VIBRATION DATA ANALYSIS

One of the challenges in conducting aerodynamic measurements for a dynamic model is removing the inertial component from the measured loads. For example, with instrumentation involving strain gauges, such as the present aerodynamic balance, measurements are a combination of the aerodynamic loads acting on the model and the inertial loads associated with the motion of the model and the balance's centre spindle to which the model is attached. Various arrangements have been used previously to remove the inertial loads. For example, a second identical "dummy" model, with its own strain gauges, may be attached to the wind tunnel model but located outside of the airflow. The "wind-off" inertial loads measured from the "dummy" model are removed from the corresponding measurements from the "wind-on" model in the tunnel [16,20]. Alternatively, a wind tunnel model incorporating an array of pressure taps may be used, where the discrete pressure readings are summed to yield the overall aerodynamic lift, drag, and moment. These previous arrangements are costly, require significant time to setup and, in the case of using pressure taps, are not well suited for a realistic iced-conductor model whose surface is irregular.

An alternative but simple strategy is taken in the present work. As Fig. 3 shows that the automated motion controls can produce repeatable motion for the wind tunnel model, each dynamic test is conducted first in still air. Then the test is repeated at the desired wind speed. The still air measurements involve only inertial loads, while a "wind-on" test includes both the inertial loads and the aerodynamic loads acting on the dynamic model. As for previous studies which used a "dummy" model, the difference between the measurements from the two tests yields just the aerodynamic loads of interest.

Preliminary forced-vibration experiments showed that the aerodynamic balance's structural vibration response was present in the measured load cell data. Therefore a straightforward modal analysis was performed on the balance to determine its natural frequencies to develop an appropriate strategy to remove the balance's contribution in the aerodynamic data. An impact hammer was used to excite the balance's side force, drag, and yawing moment channels, and the free-vibration response after the impact was measured directly using the balance's load cells.

The results of the modal analysis showed that the balance's lowest natural frequencies were surprisingly lower than expected for a general purpose instrument; approximately 11Hz for the lift, 26Hz for the moment, and 83Hz for the drag. However, as the frequency range of interest in the present experiments is about 5Hz and lower, a digital low-pass filter was used in the post-processing stage to remove essentially all the effects of the balance's structural vibrations. MATLAB's Decimate function [30] was used to decrease the sampling rate of the data from 2000Hz to 80Hz, while a suitable digital low-pass filter with a roll-off region in the range of 5-10Hz was implemented using the MATLAB filter-design toolbox [31].

In addition to the structural response of the aerodynamic balance, preliminary data showed unwanted harmonic components introduced from the stepper motor. For example, the aerodynamic data from a 1Hz forced-vibration test contained an expected 1Hz frequency component in addition to minor harmonic components at 2, 3, 4Hz and so on. The discrete nature of the operation of the balance's stepper motor caused these harmonics to appear in the load cell measurements. To remove these motor harmonics and reduce experimental error in the aerodynamic data, a motor isolation strategy and replacement servomotor were considered. These alternatives were not implemented, however, due to the significant time needed to realign and recalibrate the aerodynamic balance after making the necessary adjustments. Instead, a simple averaging scheme was developed to minimise the effect of the stepper motor's harmonics on the aerodynamic data.

Due to the repeatable nature of the balance's automated controls, the cosine motion of the wind tunnel model can repeated over an arbitrary number of cycles. In the post-processing stage, the measured aerodynamic loads over multiple cycles can be summed and then divided by the number of cycles to yield an average result. Figure 5, in which the aerodynamic loads are plotted versus normalised time, shows the superimposed aerodynamic data from about 40 cycles of a 3.2Hz, ±20° steady-state cosine motion. Note that the time is simply normalised by the periodicity of motion, T_0. The average results and approximate distributions of the experimental data are also shown for comparison. As the distributions are approximately normal, the averaging strategy appears to be fairly reasonable, and the average aerodynamic loads seem to be representative of the overall collection of data from multiple cycles.

The forced-vibration test associated with Fig. 5 was repeated to confirm the repeatability of the previously averaged aerodynamic results. Figure 6 shows the separately averaged aerodynamic loads for the separate tests. From Fig. 6, the average lift and drag results from the two individual tests indicate reasonably good agreement i.e. to within less than 0.01 and 0.02, respectively. These levels of agreement should be sufficient for identifying trends and performing relative comparisons between tests for the lift and drag coefficients. On the other hand, the average moment results given in Fig. 6 show a significant discrepancy between the two nominally identical tests. Although the motion of the wind tunnel model in both tests is accurate to ±0.2°, even such small variations may be the cause of the distinctly different aerodynamic moments. This comparison demonstrates the sensitive nature of the aerodynamic moment and the experimental difficulties in its measurement. Although the aerodynamic moment data from the dynamic tests are not repeatable, they are included subsequently for completeness.

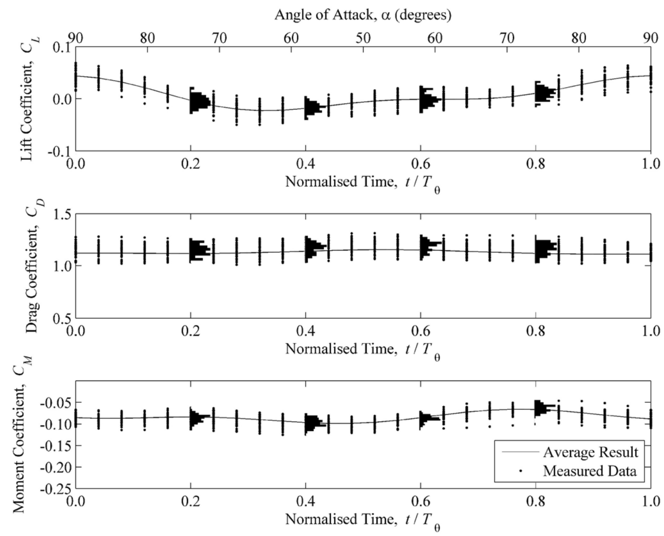

FIGURE 5. SUPERIMPOSED AERODYNAMIC DATA, APPROXIMATE MEASUREMENT DISTRIBUTIONS, AND AVERAGE RESULTS FOR A 3.2HZ, ±20° STEADY-STATE COSINE MOTION.

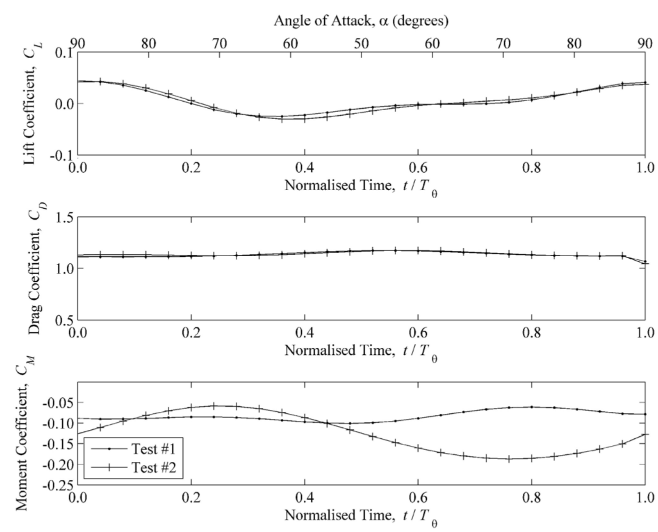

FIGURE 6. COMPARISON OF THE AVERAGE RESULTS FROM THE REPEATED FORCED-VIBRATION TEST EXAMPLE IN FIG. 5.

EXPERIMENTAL RESULTS

Quasi-Steady Results

The results from quasi-steady testing are presented in Fig. 7, where the normalised aerodynamic loads are plotted versus angle of attack for wind speeds of 10, 14, and 18m/s. Taking the bare conductor diameter, d, of 28.6mm as a characteristic length scale, these wind speeds correspond to Reynolds Numbers, *Re,* of about 18200, 25500, and 32700, respectively. The Reynolds Number is defined here as

$$Re = \frac{V\,d}{\nu} \tag{6}$$

where ν is the kinematic viscosity of air.

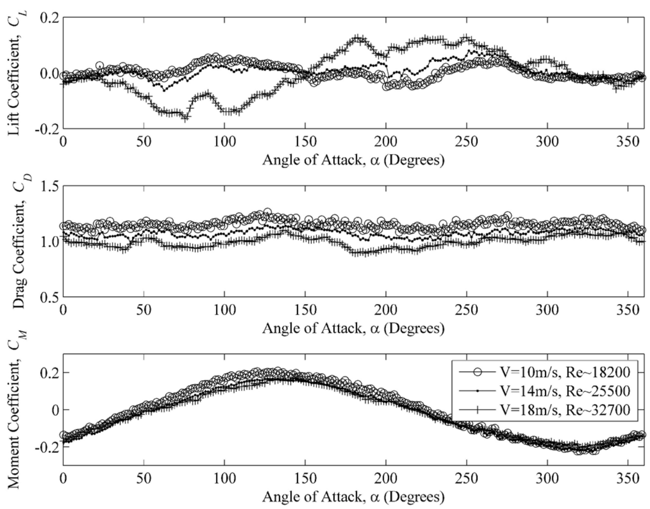

FIGURE 7. QUASI-STEADY RESULTS FOR WIND SPEEDS OF 10, 14, AND 18m/s.

The lift and drag data in Fig. 9 are fitted with cubic polynomials to determine if the den Hartog criterion (1) is satisfied. While a cubic polynomial does not provide a good approximation of the data over the entire range of 360°, a fairly reasonable approximation is achieved by considering intervals of 30°. The experimental lift, drag and their cubic fits as well as the value of the den Hartog criterion are presented in Figs. 8 through 10 for the three wind speeds.

The effects of wind speed are seen in the quasi-steady lift and drag results presented in Fig. 7. As the wind speed increases from 10 to 18m/s, the peak-to-peak level and slopes of the quasi-steady lift curve become larger, while the drag curve decreases from about 1.2 to 1.0. These changes generally lead to a greater possibility of satisfying the den Hartog criterion for vertical galloping. The wind speed or Reynolds Number effects also help explain the disagreement in the literature regarding lightly-iced conductor profiles and the den Hartog criterion. For example, Tunstall's study [12], which was conducted at about 18m/s with a slightly thicker ice accretion, showed that lightly-iced conductors satisfy the den Hartog criterion. In contrast, Ontario Hydro's tests [8,9] were conducted at somewhat lower 8 and 12m/s wind speeds. They showed that the den Hartog criterion is not satisfied at any angle of attack. The present aerodynamic data and den Hartog results, which are shown in Figs. 8 through 10 for steady wind speeds between 10 and 18m/s, support the conclusion of Ontario Hydro. The value of the den Hartog is always positive, implying that the profile is vertically stable. Therefore the common case of lightly-iced conductor galloping observed in the field cannot be explained by a simple vertical instability and additional mechanisms must be involved.

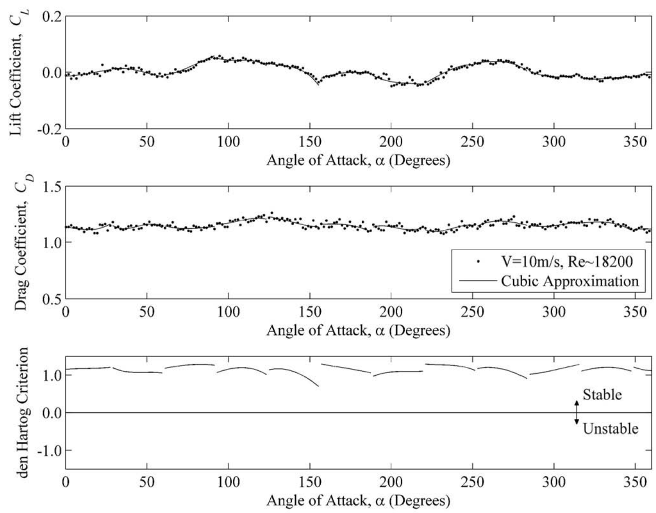

FIGURE 8. QUASI-STEADY LIFT, DRAG, AND DEN HARTOG RESULTS MEASURED AT 10m/s.

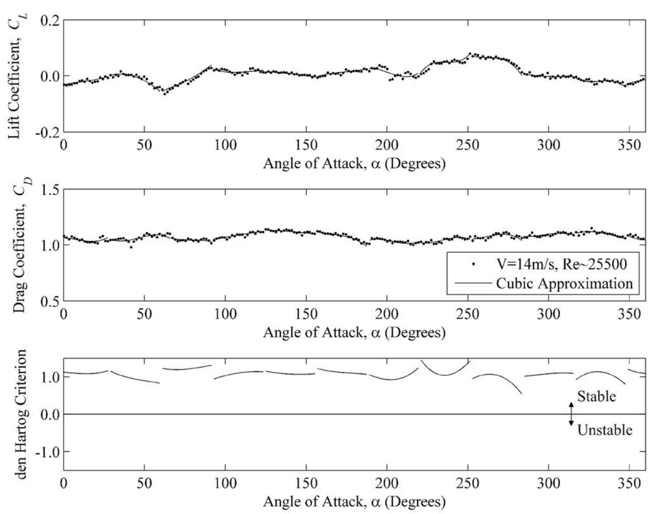

FIGURE 9. QUASI-STEADY LIFT, DRAG, AND DEN HARTOG RESULTS MEASURED AT 14m/s.

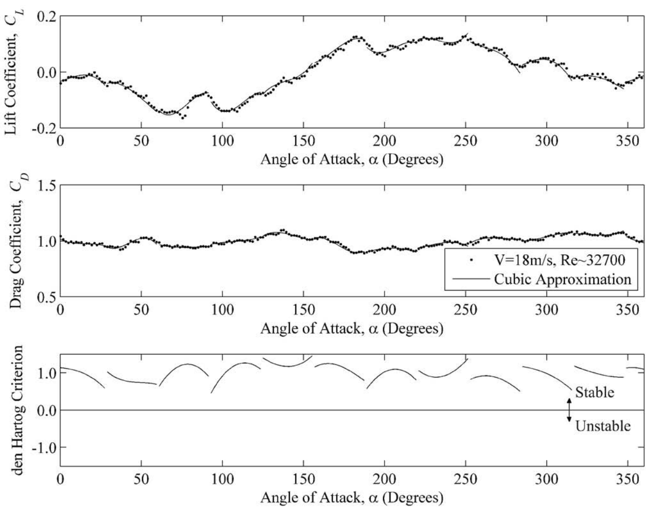

FIGURE 10. QUASI-STEADY LIFT, DRAG, AND DEN HARTOG RESULTS MEASURED AT 18m/s.

Forced-Vibration Results

The dynamic test results for various rotational frequencies, an initial angle of attack of 35°, and a steady-state rotational amplitude of 5° are presented in Fig. 13. The aerodynamic loads measured in each dynamic test are superimposed in Fig. 11 along with the quasi-steady aerodynamic loads measured over the same angles of attack. Figure 12 shows the results from additional testing performed with a rotational amplitude of 20°, while Fig. 13 presents results for an initial angle of attack of 70° and a steady-state rotational amplitude of 20°. The wind speed for all of the results presented in Fig. 11 through 13 is 10m/s.

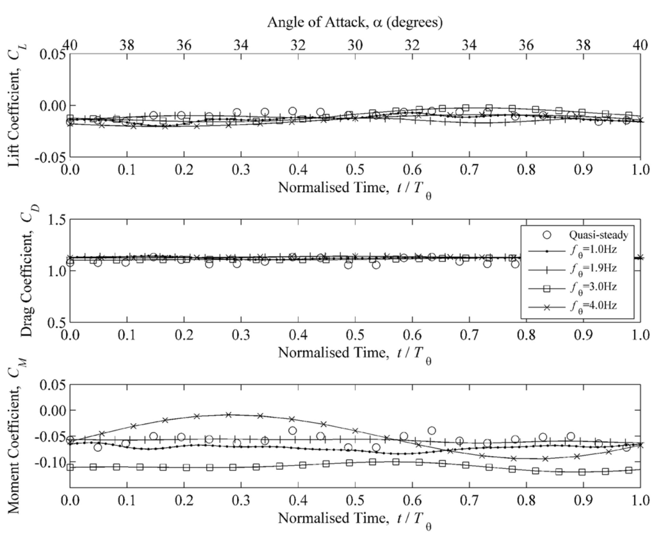

FIGURE 11. QUASI-STEADY AND FORCED-VIBRATION RESULTS MEASURED AT 10m/s, WHERE α_0=35° and A_θ=5°.

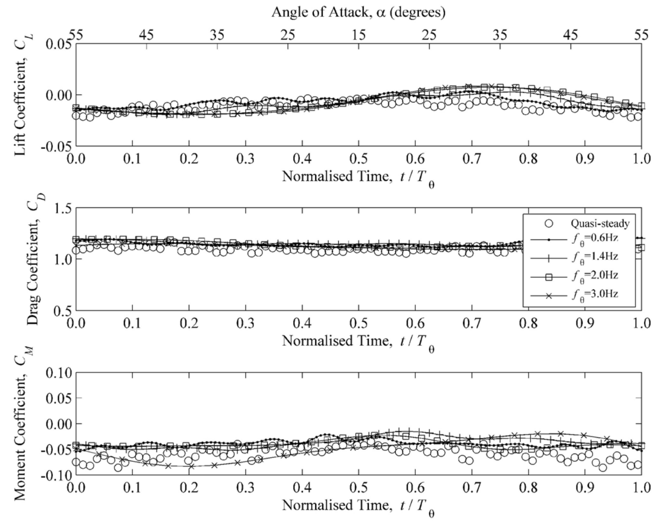

FIGURE 12. QUASI-STEADY AND FORCED-VIBRATION RESULTS MEASURED AT 10m/s, WHERE α_0=35° and A_θ=20°.

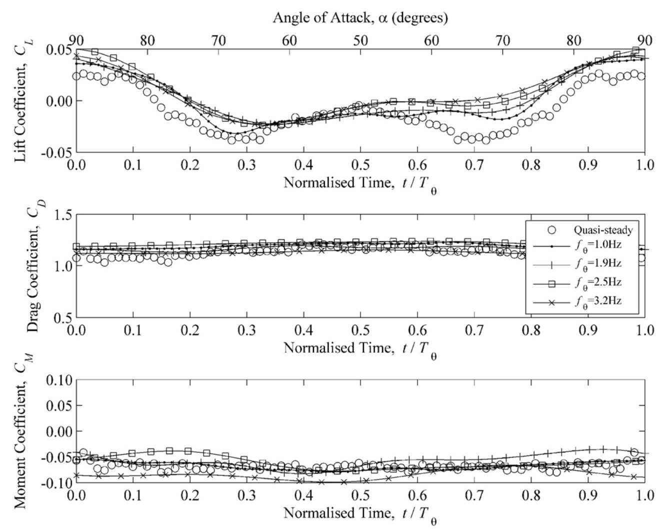

FIGURE 13. QUASI-STEADY AND FORCED-VIBRATION RESULTS MEASURED AT 10m/s, WHERE α_0=70° and A_θ=20°.

Effects of Rotational Amplitude. A comparison of the 3.0Hz dynamic test results given in Figs. 11 and 12 shows that, as the rotational amplitude increases from ±5° to ±20°, deviations from the quasi-steady lift become slightly more evident. Although these changes are subtle and within the uncertainty of the measurements before averaging, they are intuitively expected. To illustrate this assertion, note that the model's maximum angular speed is simply proportional to the product of the rotation's frequency and peak amplitude. At low rotational amplitudes, such as the ±5° data presented in Fig. 11, relatively good agreement is seen between the quasi-steady lift and drag and the corresponding dynamic test results. These data suggest that the use of quasi-steady theory around the onset of galloping is appropriate. However, as galloping motions grow and rotations become larger in amplitude, corresponding, to say, the ±20° data shown in Fig. 12, the quasi-steady theory and characteristic radius approach are unable to account for changes in the lift force arising from the rotational motion. The significance of this additional rotation-induced lift force is examined more closely next.

Effects of Rotational Frequency. Figures 12 and 13 show that as the rotational frequency increases, but the rotational amplitude is fixed at ±20°, the drag force always remains consistent with its corresponding quasi-steady values. On the other hand, the dynamic lift force measurements tend to deviate away from their quasi-steady values. These deviations are likely induced by the rotational motion. As the model follows a periodic cosine profile, the rotational motion is counter-clockwise, but clockwise in the first and second half of the cycle, respectively. Figure 12 show that when the quasi-steady lift is practically flat or insensitive to changes in angle of attack, the additional lift caused by the counter-clockwise motion is negative in the first half of the cycle, but positive in the second half cycle. These results agree with the classical theory for spinning cylinders, in which clockwise and counter-clockwise rotations produce positive and negative lift forces, respectively [32].

Figures 12 and 13 further show that the lift deviations from their quasi-steady values are more noticeable in the second half of the cosine motion. This result is most likely caused by a short-term fluid-memory effect, similar to that observed by Nakamura [20]. The model's surrounding airflow begins to compensate the counter-clockwise rotation, but is then perturbed further by the immediately following clockwise motion. However, because the model is forced by the automated controls to remain in a repeatable, steady-state motion, any possible fluid-memory effects are not allowed to buildup in subsequent cycles of the oscillation. A spring-supported model may be useful to examine any fluid-memory effects more closely in future studies, again. Such models can allow the rotational motion to slowly buildup under unstable conditions, thereby allowing any fluid-memory effects to also buildup with increasing rotational amplitude.

The relatively low 0.6Hz rotational test results given in Fig. 12 show reasonable agreement with the quasi-steady lift and drag. However, the lowest natural torsional frequency of a typical lightly-iced transmission is usually several times higher than 0.6Hz [4]. The torsional frequency may gradually decrease to around 0.6Hz with increasing icing and time [2]. The dynamic results suggest that a rotational oscillation at these initially higher frequencies may produce a periodic lift force which is superimposed on the quasi-steady lift. This type of aerodynamic coupling phenomenon may be an important aerodynamic mechanism acting in the galloping of lightly-iced transmission lines. Such a linking of the rotational and vertical DOFs has been suspected in previous studies, although only numerical simulations were performed [15]. Note that the repeatability of the present results has been confirmed when averaging over about 40 cycles of motion. However, the relatively high levels of uncertainty in the basic measurement data should be addressed to establish more confidence in the present findings. A simple but custom-built aerodynamic balance designed for more sensitive lift measurements is needed.

Effects of Initial Angle of Attack. A comparison of Figs. 12 and 13 shows that both the quasi-steady and dynamic lift results depend strongly on the initial angle of attack. For example, in the case when α_0 is 70°, as shown in Fig. 13, the quasi-steady lift exhibits a relatively steep positive slope. This behaviour suggests that the airflow's separation points and the ensuing flow field around the iced conductor are quite sensitive to rotations and changes in the model's angle of attack. This behaviour is confirmed in subsequent visualisations. The increased sensitivity of the flow field in this region results in higher deviations from the quasi-steady lift found in Fig. 13. In regions where the lift curve is relatively flat, such as in Fig. 12, a rotation-induced lift is still seen in the dynamic results, although not to the same extent as that observed in Fig. 13. In such cases, the flow field is suspected to be less sensitive to changes in the angle of attack and the rotational motion. These results have important implications as the den Hartog explanation of iced-conductor galloping has been based upon regions where the quasi-steady lift curve is steep and negative. The present results suggest that such regions, as well as those featuring positive lift slopes, exhibit the most noticeable deviations from the quasi-steady theory. These deviations may lead to stronger galloping behaviour due to the increased coupling between the rotational and vertical DOFs.

Visualisation Results

Visualisations from the quasi-steady testing are superimposed in Fig. 14. For each individual visualisation image, a label is used to show the airflow's separation point location at the surface of the model. The images are superimposed together for comparison purposes and to track any subtle changes in the separation points. The static angle of attack in Fig. 14 is changed from 50° to 90° in increments of 10°. This range of angles coincides with a relatively steep quasi-steady lift curve given in Fig. 13. (A steep lift curve implies that the lift is sensitive in this region to small changes in the angle of attack.) The most significant deviations from the quasi-steady lift values are also seen in this range.

The visualisations from the 3.2Hz dynamic test, which corresponds to the data of Fig. 13, are also incorporated in Fig. 15 for the 70° angle of attack. Only visualisations the "upper" separation point are shown for brevity. They identify the instants when the model undergoes a clockwise (CW) and a counter-clockwise (CCW) rotation. The flow's "upper" separation point location from the (static) quasi-steady visualisations is also included for comparison. Only the 70° angle of attack is shown here as this angle corresponds to the instant of maximum rotational speed.

The visualisations of the quasi-steady results, which are superimposed in Fig. 14, indicate that relatively small surface irregularities of an icing have a surprisingly noticeable effect on the conductor's "upper" separation point. However, on the "lower" stranded surface of the conductor where little to no icing is present, the "lower" separation point's location hardly changes over the entire 40° range considered. These results strongly support Tunstall's position [12] that previously used, ideal smooth models are unrepresentative of "naturally" iced conductors. Furthermore, Fig. 15 shows that the changes in the "upper" separation point location due to the surface irregularities of ice are further exaggerated by rotational motion. The more noticeable shift in the "upper" separation point's location during a clockwise motion supports the previous aerodynamic data in which clockwise motions result in greater deviations from quasi-steady values.

These visualisations suggest that both the irregular surface geometry of ice as well as rotational motion contribute to the aerodynamic coupling effects observed in the aerodynamic measurements. However, further visualisations and aerodynamic measurements are needed to corroborate the present results.

(a)

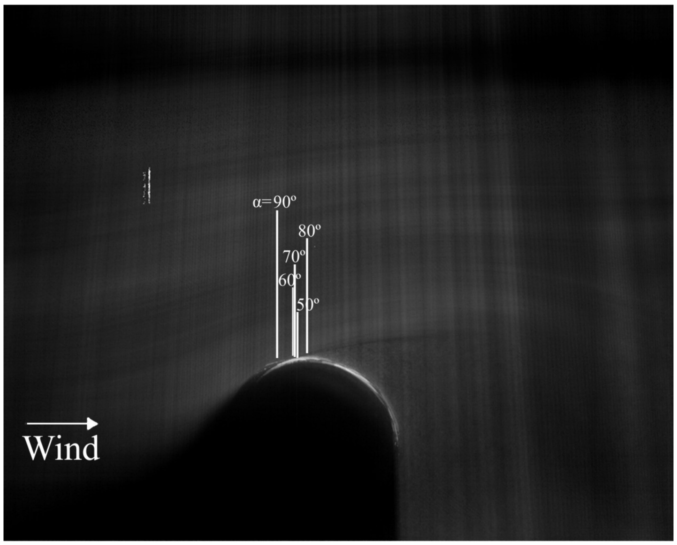

(b)

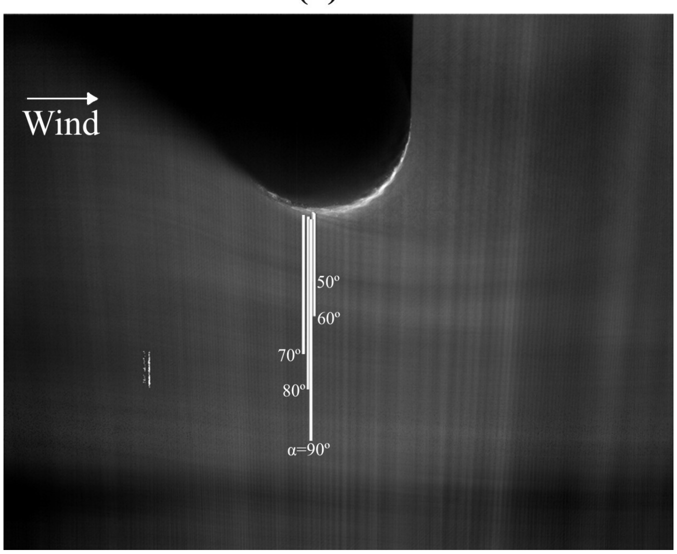

FIGURE 14. SUPERIMPOSED QUASI-STEADY VISUALISATION RESULTS FOR THE MODEL'S (a) "UPPER" AND (b) "LOWER" SEPARATION POINTS.

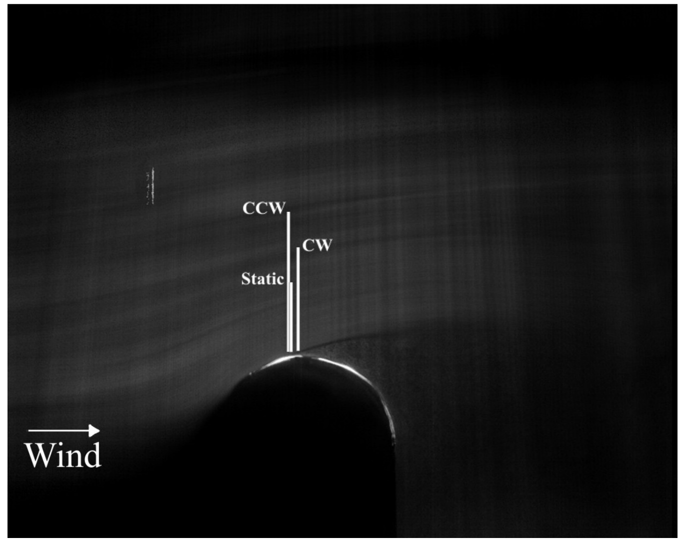

FIGURE 15. SUPERIMPOSED DYNAMIC VISUALISATION RESULTS SHOWING THE MODEL UNDERGOING COUNTER-CLOCKWISE (CCW) AND CLOCKWISE (CW) MOTION FOR THE INSTANT WHEN α=70°.

CONCLUSIONS

Quasi-steady wind tunnel testing has shown that the well-established den Hartog criterion for vertical galloping predicts stable conditions at all angles of attack for a typical, lightly-iced conductor. Therefore lightly-iced conductor galloping, which is observed commonly in the field, cannot be explained by a simple vertical instability.

A lightly-iced conductor model undergoing prescribed 1-DOF rotational oscillations has been used to examine the possible effects of a rotational motion on the aerodynamic loads in conductor galloping. The drag is essentially identical to its quasi-steady counterpart. However, differences in the dynamic lift became more noticeable at higher rotational frequencies and amplitudes.

Visualisation images showed that the location of the airflow's separation point on the "upper" iced portion of the conductor, unlike that on the "lower" bare portion, is affected by minor ice surface irregularities. This results in a rotation-induced lift. Further 2-DOF studies are needed to fully assess its influence.

ACKNOWLEDGEMENTS

Mr. D. Stoyko and Mr. V. Stoyko are acknowledged for their efforts in helping to prepare the wind tunnel experiments. Financial support for the present work is provided by the Natural Science and Engineering Research Council.

REFERENCES

[1] Electric Power Research Institute (EPRI), 1979. *Transmission Line Reference Book, Wind-Induced Conductor Motion*. Palo Alto, California.

[2] Cigré Task Force B2.11.06, 2005. *State of the Art of Conductor Galloping*, Hydro Quebec - IREQ, Quebec, Canada.

[3] Edwards, A.T. and Madeyski, A., 1956. "Progress Report on the Investigation of Galloping Transmission Line Conductors". *Tr. AIEE*, Vol. 75, p.666-686.

[4] Nigol, O. and Clarke, G.J., 1974. "Conductor Galloping and Control Based on Torsional Mechanism". *IEEE Pwer Engng. Society Meeting*, Paper No. C74 016-2, New York.

[5] Van Dyke, P. and Laneville, A., 2008. "Galloping of a Single Conductor Covered with a D-Section on a High-Voltage Overhead Test Line". *Journal of Wind Engineering and Industrial Aerodynamics,* Vol. 96, p.1141-1151.

[6] Lilien, J.L. and Havard, D.G., 2000. "Galloping Data Base on Single and Bundle Conductors. Prediction of Maximum Amplitudes". *IEEE Trans on Power Delivery,* Vol. 15 (2), p.670-674.

[7] Chadha, J., 1974. "A Dynamic Model Investigation of Conductor Galloping". *IEEE Winter Power Meeting*, Paper 74 59-2.

[8] Nigol, O. and Buchan, P.G., 1981. "Conductor Galloping Part I - Den Hartog Mechanism". *IEEE Trans. PAS*, Vol. 96 (2), p.699-707.

[9] Nigol, O. and Buchan, P.G., 1981. "Conductor Galloping Part II - Torsional Mechanism". *IEEE Trans. PAS*, Vol. 96 (2), p.708-720.

[10] Chabert, O. and Lilien, J.L., 1998. "Galloping of Electrical Lines in Wind Tunnel Facilities". *Journal of Wind Engineering*, Vol. 74-76, p.967-976.

[11] Stumpf, P., 1994. "Determination of Aerodynamic Forces for Iced Single and Twin-Bundled Conductors". *M.Sc. Thesis*, University of Manitoba, Winnipeg, Canada.

[12] Tunstall M.J. 1989. "Accretion of Ice and Aerodynamic Coefficients". *Presentation to the AIM Study Day on Galloping*, University of Liege.

[13] Richardson, A.S., 1981. "Dynamic Analysis of Lightly Iced Conductor Galloping in Two Degrees of Freedom". *Proc. IEEE*, Vol. 128 (Pt. C) (4), p.211-218.

[14 Den Hartog, J.P., 1947. *Mechanics of Vibrations.* McGraw-Hill Book Company Inc., New York, NY.

[15] McComber, P., and Paradis, A., 1998. "A Cable Galloping Model for Thin Ice Accretions". *Journal of Atmospheric Research*, Vol. 46, p.13-25.

[16] Washizu, K., Ohya, A., Otsuki, Y., and Fujii, K., 1980. "Aeroelastic Instability of Rectangular Cylinders in a Torsional Mode due to a Transverse Wind". *Journal of Sound and Vibration*, Vol. 72 (4), p.507-521.

[17] Cheers, F., 1950. "A Note on Galloping Conductors". *Report MT-14*. National Research Council, Ottawa.

[18] Chan, J.K., Shah, A.H., and Popplewell, N., 1992. *Modelling of Conductor Galloping*. Canadian Electrical Association, Project 321 T 672.

[19] Blevins, R.D. 1990. *Flow-Induced Vibration (2nd Edition)*. Van Nostrand Reinhold Co., New York.

[20] Nakamura, Y., 1979. "On the Aerodynamic Mechanism of Torsional Flutter of Bluff Structures". *Journal of Sound and Vibration*, Vol. 67, p.163-177.

[21] Nakamura, Y. and Mizota, T., 1975. "Torsional Flutter of Rectangular Prisms". *Journal of the Engineering Mechanics Division,* Vol. 101 (2), p.125-142.

[22] Waris, M.B., Ishihara, T., and Sarwar M.W., 2008. "Galloping Response Prediction of Ice-Accreted Transmission Lines". *The 4th International Conference on Advances in Wind and Structures*, Korea.

[23] Wang, J. and Lilien, J.L., 1998. "Overhead Electrical Transmission Line Galloping: A Full Multi-Span 3-DOF Model, Some Applications, and Design Recommendations". *IEEE Transactions on Power Delivery*, Vol. 13, p.909-916.

[24] Stumpf, P. and Ng, H.C.M., 1990. "Investigation of Aerodynamic Stability for Selected Inclined Cables and Conductor Cables". *B.Sc. Thesis*, University of Manitoba, Winnipeg, Canada.

[25] Zan, S.J., Wardlaw, R.L., and Stumpf, P., 1993. "Wind Tunnel Tests of an Iced Bundled- Conductor Model". *Proceedings of the 14th Canadian Congress on Applied Mechanics*.

[26] Fujisawa, N., Ikemoto, K., and Nagaya, K., 1998. "Vortex Shedding Resonance from a Rotationally Oscillating Cylinder". *Journal of Fluids and Structures*, Vol. 12, p.1041-1023.

[27] Zdero, R., Turan, O.F., and Harvard, D.G., 1995. "Toward Understanding Galloping: Near-Wake Study of Oscillating Smooth and Stranded Circular Cylinders in Forced Motion". *Experimental Thermal and Fluid Science*, Vol. 10 (1), p.28–43.

[28] Mejia, K.M. and Jorgens, C.J. 2007. "Conceptual Design of a Laser Light Sheet Flow Visualization System for a Pressurized, Low Speed Wind Tunnel". *22nd International Congress on Instrumentation in Aerospace Simulation Facilities*, p.1-13.

[29] Akbel, V.D., 2005. "Aerodynamic Data for Iced Power Line Samples," *M. Eng. Report.* University of Manitoba, Winnipeg, Canada.

[30] The MathWorks Inc., 2010. Decimation - decrease sampling rate - MATLAB. On the WWW, January. URL http://www.mathworks.com/access/helpdesk/help/toolbox/signal/decimate.html

[31] The MathWorks Inc., 2010. Filter Design Toolbox - Documentation. On the WWW, January. URL http://www.mathworks.com/access/helpdesk/help/toolbox/filterdesign/

[32] Goldstein S., 1956. *Modern Developments in Fluid Dynamics, Vol. II.* Dover Publications, New York.